Journal of Power Sources 238 (2013) 464–468

Contents lists available at SciVerse ScienceDirect

Journal of Power Sources

journal homepage: www.elsevier.com/locate/jpowsour

Short communication

The preparation of double-void-space SnO_2/carbon composite as high-capacity anode materials for lithium-ion batteries

Wenchao Wang, Penghui Li, Yanbao Fu, Xiaohua Ma*

Department of Materials Science, Fudan University, Shanghai 200433, People's Republic of China

HIGHLIGHTS

- We designed a new nanostructure: double-void-space SnO_2/carbon composite.
- We used modified Stöber method to get satisfied thickness of SiO_2 layer.
- The large void space made the materials to have sufficient physical buffer zones.
- The composite displayed satisfied results in performance of capacity and cycle life.

ARTICLE INFO

Article history:
Received 29 October 2012
Received in revised form
6 April 2013
Accepted 8 April 2013
Available online 24 April 2013

Keywords:
Tin dioxide/carbon composite
Tin dioxide hollow spheres
Double-void-space
High capacity

ABSTRACT

In this work, double-void-space SnO_2/carbon composite has been synthesized as high-capacity anode materials for lithium-ion batteries. This novel designed structure, with the internal void space inside SnO_2 hollow spheres and the external void space between SnO_2 and carbon, can superiorly accommodate the large volume change as a physical buffering layer during the charge/discharge procedure. It is found that the double-void-space SnO_2/carbon composite manifest a much higher reversible capacity compared to SnO_2 hollow spheres. Due to the formation of the void space, the special composite is able to deliver a reversible Li storage capacity of 408.4 mAh g^{-1} after 50 cycles. This implies the structural optimization can provide new opportunities to enhance the properties of tin-based materials for high-capacity lithium-ion batteries.

© 2013 Elsevier B.V. All rights reserved.

1. Introduction

Lithium ion batteries (LIBs), as one of the most promising candidates for electrochemical energy conversion and storage devices, have attracted much attention in the scientific and industrial fields due to their high energy density [1]. The increasing demands for electrode materials, especially with high capacity and long cycle life, have prompted numerous research efforts in recent years [2,3]. Some promising negative materials such as silicon (Si), tin (Sn), Fe_3O_4, Co_3O_4 and SnO_2 have attracted much interest because of their much higher specific lithium storage capacity than the graphite materials [4–8]. In particular, tin-based materials have been intensively studied due to their large theoretical specific capacities (990 mAh g^{-1} for Sn; 779 mAh g^{-1} for SnO_2), which is much higher than the currently used graphite materials (372 mAh g^{-1}) [9,10]. However, the most serious problem of tin-based anodes is the huge volume change (more than 200%) during Li^+ insertion and extraction [11], which caused disintegration and pulverization of the electrodes. Therefore, the volume change leads the tin-based materials to very rapid capacity decay [1].

To solve this so-called "pulverization" problem, many research papers were focused on producing a buffering layer or void space for Sn/SnO_2. Hollow nanostructures (nanospheres [12], nanotubes [13] and nanoboxes [14]) are synthesized in order to have the interior void spaces, which could partially accommodate the large volume change. Another commonly approach is to make composite materials with carbon (carbon [15,16], carbon nanotube [17,18] and graphene [19]), where carbon provides a high surface area, a physical buffering layer and a perfect electrical conductivity [20–22]. For example, Wang et al. demonstrated a facile template chemical vapor deposition (CVD) method to produce CNT-encapsulated Sn nanoparticles with ~100% particle encapsulation and high filling uniformity. The completely filled Sn@CNT nanocomposite showed excellent reversible lithium ion storage properties [17]. Zhang et al. designed a new approach to prepare tin

* Corresponding author. 220 Handan Road, Shanghai 200433, People's Republic of China. Tel./fax: +86 021 55664024.
E-mail address: xhma@fudan.edu.cn (X. Ma).

0378-7753/$ – see front matter © 2013 Elsevier B.V. All rights reserved.
http://dx.doi.org/10.1016/j.jpowsour.2013.04.023

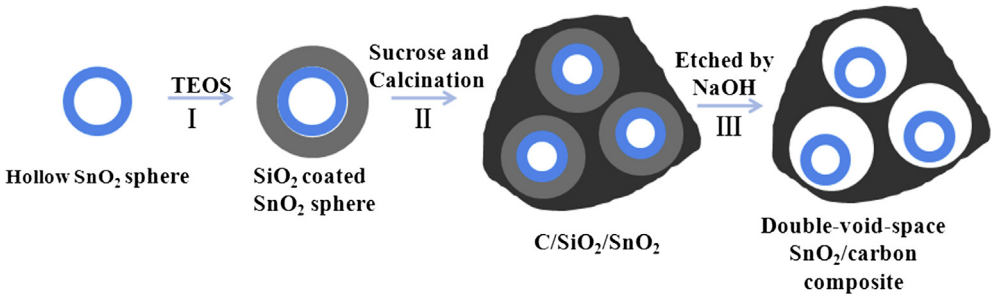

Fig. 1. Synthetic scheme of double-void-space SnO_2/carbon composite.

nanoparticles encapsulated elastic hollow carbon spheres, which showed high volume capacity and good cycle performance [23]. It is obvious that the "void spaces" place a very important role in tin-based materials for the high-capacity lithium ion batteries. However, it is still a great challenge to explore an effective and facile route for designing the composites.

Herein, we design a new nanostructure for anode materials: double-void-space SnO_2/carbon composite. The synthetic procedure of SnO_2/carbon composite is schematically illustrated in Fig. 1. We prepared the SnO_2 hollow spheres by a simple one-pot template-free synthesis, based on an unusual inside-out Ostwald ripening mechanism. In step I, the mesoporous SnO_2 was encapsulated by SiO_2 with the modified Stöber method to get the satisfied thickness [24]. After step II and III, the double-void-space SnO_2/carbon composite showed not only the internal void space inside the SnO_2 hollow spheres but also the exterior void space between SnO_2 and synthesized carbon. With the novel structure we can overcome the major disadvantages of "pulverization" problem for poor cycling performance so as to provide excellent electrochemical properties.

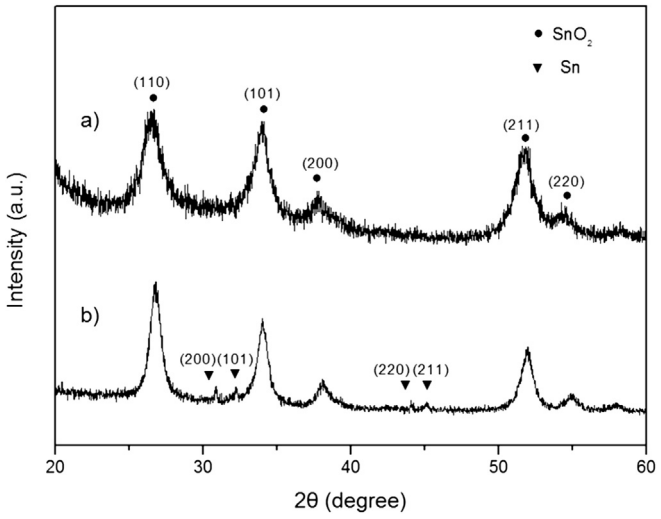

Fig. 2. Powder XRD patterns for (a) SnO_2 and (b) double-void-space SnO_2/carbon composite.

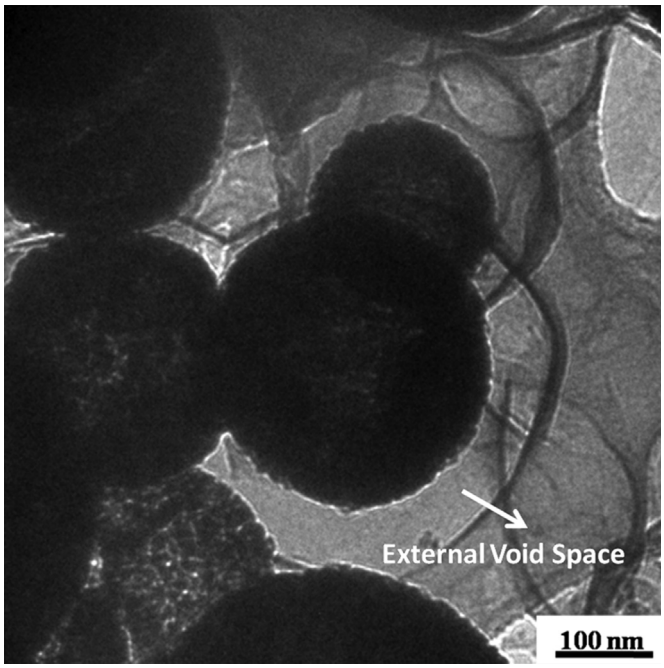

Fig. 4. HRTEM images for double-void-space SnO_2/carbon composite.

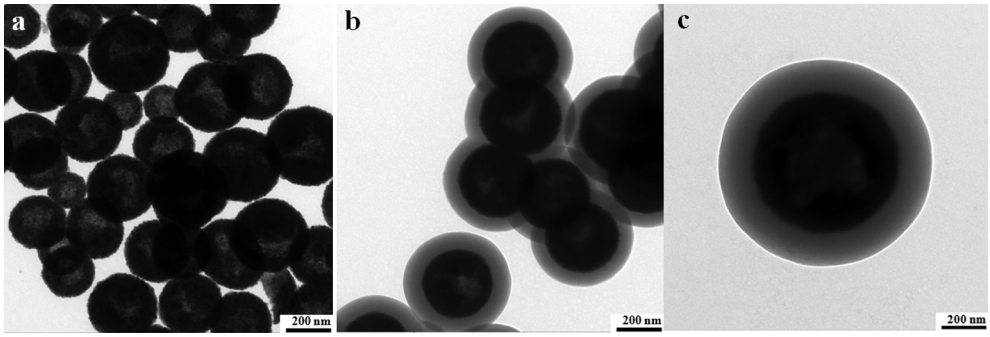

Fig. 3. (a) TEM image of SnO_2 hollow spheres, (b, c) TEM images of SiO_2 coated SnO_2 spheres.

2. Experimental

2.1. Synthesis of double-void-space SnO_2/carbon composite

All the chemicals are analytic grade, and used as received. The SnO_2 hollow spheres were prepared through a hydrothermal route: typically a mixture of potassium stannate trihydrate ($K_2SnO_3 \cdot 3H_2O$, Aldrich, 99.9%) and urea were dissolved in a mixed solvent of ethanol/water (37.5% ethanol by volume) to achieve concentrations of 16 mM and 0.1 M, respectively. The resulting solution was then transferred into a 100 ml Teflon lined stainless steel autoclaves, and heated at 200 °C for 24 h. After cooling to room temperature, the white precipitate was obtained by centrifugation, and then washed for at least five times with distilled water followed by vacuum drying at room temperature [25].

To prepare SiO_2/SnO_2 composite, 0.2 g of as-synthesized SnO_2 hollow spheres were easily dispersed in a mixture solvent of water/ethanol/isopropanol/n-butanol (20 ml/50 ml/50 ml/50 ml). Then 1 ml of tetraethyl orthosilicate (TEOS) and 8 ml concentrated ammonia solution (37 wt%) were added dropwise during a period of 2 h and the reaction was allowed to proceed for 24 h under continuous mechanical stirring. The resultant product was separated and collected by centrifugation and washed with ethanol for several times followed by drying in a vacuum oven at 60 °C for 12 h.

In a typical procedure, 0.5 g of sucrose, 0.2 g of H_2SO_4 and 10 g H_2O were infiltrated with 1.0 g of SiO_2/SnO_2 composite, then dried in the oven at 80 °C for 6 h, followed at 160 °C for another 6 h. This infiltration and drying procedure was repeated once. The obtained sample was calcined at 700 °C for 3 h in N_2 atmosphere for complete carbonization. The as-prepared $C/SiO_2/SnO_2$ composite was dispersed in 2 M NaOH solution under mild stirring for 12 h to remove the middle layer of SiO_2 [26].

2.2. Structure and electrochemical characterization

Power X-ray diffraction (XRD) was obtained by a Rigaku D/max-γB X-ray diffractometer with Cu Kα irradiation ($\lambda = 1.5418$ Å) at 40 kV and 100 mA.

Thermogravimetric analysis (TGA) was conducted with Netzsch TG 209F1 that was fitted to an air purge gas at 5 °C min^{-1} heating rate.

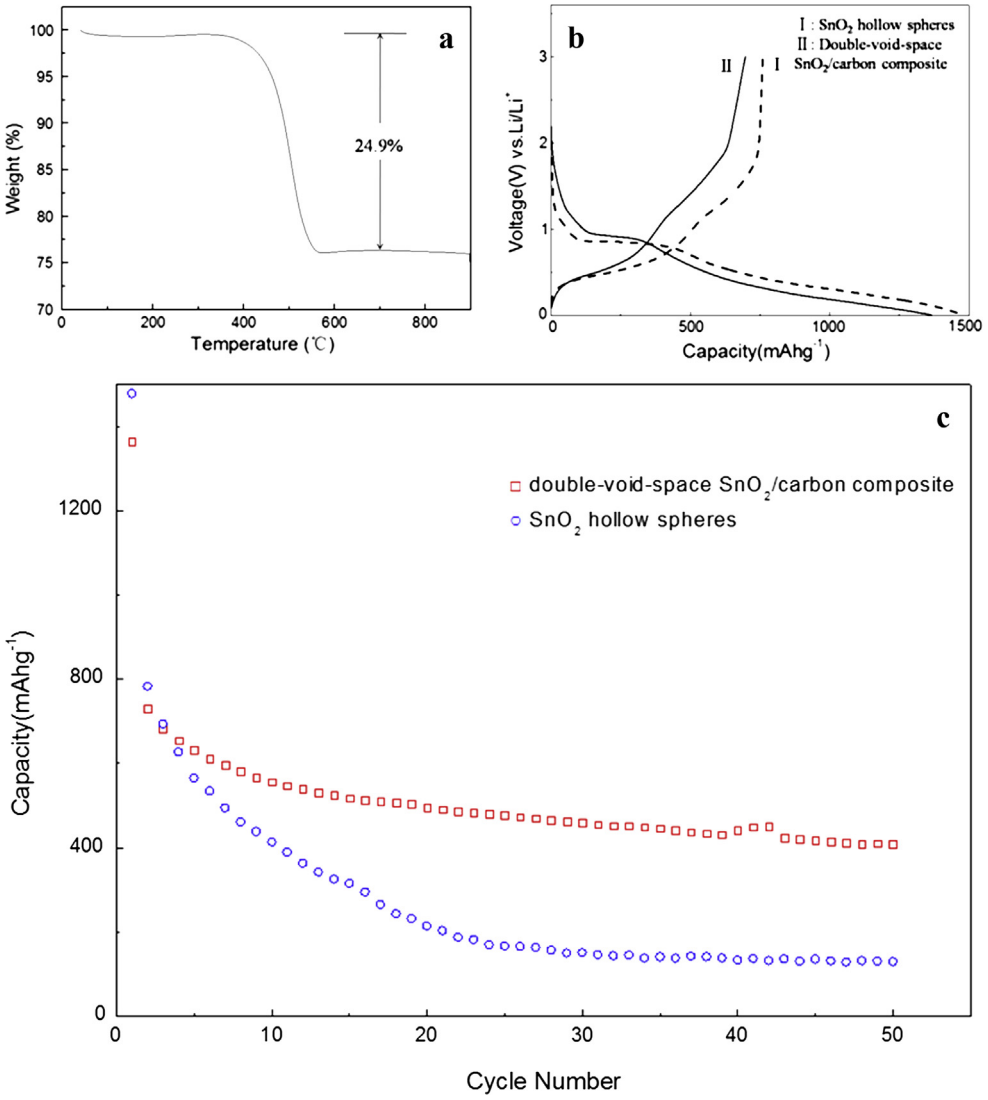

Fig. 5. (a) TGA curve under air with a ramp of 10 °C min^{-1}, (b) typical discharge–charge voltage profiles of SnO_2 hollow spheres (including the carbon black) and double-void-space SnO_2/carbon composite (including the carbon black and the carbon materials of SnO_2/carbon composite) at a current density of 100 mA g^{-1}, (c) cycling performance of SnO_2 and SnO_2/carbon composite at a current density of 100 mA g^{-1}.

Transmission electron microscope (TEM) observation was acquired using a JEM-2100 (JEOL Japan). High-resolution transmission electron microscope (HRTEM) images were obtained by a JEM-2100F (JEOL, Japan) field emission transmission electron microscope operated at accelerating voltage of 200 kV.

For electrochemical characterization, the electrode was prepared as follows: a mixture of 80 wt% double-void-space SnO_2/carbon composite, 10 wt% polyvinylidinedifluoride (PVDF) and 10 wt% carbon black was dissolved in N-methylpyrrolidone (NMP) with a mild stirring for 3 h. Then the slurry was coated onto a copper foil current collector with a blade. The electrode was dried for 12 h at 130 °C in a vacuum oven. Lithium metal foil was used as the anode and a Celgard 2400 was used as a separator. The electrolyte was composited of 1 M $LiPF_6$ in ethylene carbonate (EC):dimethyl carbonate (DMC):diethyl carbonate (DEC) (1:1:1, *v*/*v*/*v*). Cell assembly was carried out in an argon-filled glove-box (with the concentrations of moisture and oxygen below 1 ppm). The electrochemical performance was tested in the voltage range of 0.005–3.00 V on LAND-CT2001A cycle life tester (Wuhan Jinnuo Electronics Co., Ltd., China).

3. Results and discussion

Fig. 2 shows the XRD pattern of the SnO_2 nanoparticles and the prepared double-void-space SnO_2/carbon composite. The chemical composition of the as-prepared SnO_2 spheres was confirmed by XRD analysis as shown in Fig. 2a. All the identified peaks of the XRD patterns can be unambiguously assigned to tetragonal SnO_2 (cassiterite, Joint Committee on Powder Diffraction Standards (JCPDS) card no. 41-1445, S.G.: $P4_2/mnm$, $a_0 = 4.7382$ Å, $c_0 = 3.1871$ Å). In Fig. 2b, we discover that there are several peaks of the metal Sn. The result implies the SnO_2 hollow spheres are slightly reduced by calcinations at 700 °C. This phenomenon may be due to the incomplete encapsulation of SnO_2/SiO_2. Some individual SnO_2 hollow spheres will be reduced by the carbon sources. Since most of the SnO_2 spheres are coated by SiO_2, the content of reduced metal Sn in the double-void-space SnO_2/carbon composite is so low that we can neglect the influence to the electrochemical performance of the sample.

The morphology and microstructure of the as-synthesized SnO_2 hollow spheres and SnO_2/carbon composite are examined with transmission electron microscopy (TEM). From the TEM image shown in Fig. 3a, the hollow structures are synthesized through the hydrolysis of $K_2SnO_3 \cdot 3H_2O$ without any template. The formation of interior void space is based on an inside-out Ostwald ripening mechanism: during the hydrothermal ripening process, the amorphous particles at the central part posses higher surface energy and thus are easier to dissolve and relocate to the outer regions, where crystallization takes place. The as-prepared SnO_2 hollow spheres have uniform size (300 nm–350 nm) and the shell thickness of about 50 nm from Fig. 3a. After a modified Stöber method, the SnO_2 spheres are encapsulated with a layer of solid SiO_2 layer of 100 nm in thickness (Fig. 3b, c). Compared to the classical Stöber method, we change solvent to the mixture of water/ethanol/isopropanol/n-butanol. The reducing of the solvent polarity can prevent the formation of pure detached SiO_2 particles and is contributed to the formation of the satisfied thickness of SiO_2.

The HRTEM images in Fig. 4 show the double-void-space of the SnO_2/carbon composite. After the silica shells were etched by a NaOH solution, the SnO_2 spheres were well embedded into the prepared carbon walls. The outer void space between SnO_2 hollow spheres and synthesized carbon can be clearly observed from Fig. 4. This new architecture of carbon walls can function as stable mechanical support for hollow SnO_2.

To determine the carbon content in the double-void-space SnO_2/carbon composite, thermogravimetric analysis (TGA) is carried out. Fig. 5a shows the TGA curve under air with a temperature ramp of 10 °C min^{-1}. The carbon is burned out below 600 °C and the content of the carbon in the composite is simply determined to be about 24.9% by weight.

Typical charge/discharge curves of samples at a constant current rate of 100 mA g^{-1} are shown in Fig. 5b. In a SnO_2/Li half cell, there are two principal electrochemical processes [22,27]:

$$SnO_2 + 4Li^+ + 4e^- \rightarrow Sn + 2Li_2O;$$

$$Sn + xLi^+ + xe^- \leftrightarrow Li_xSn \ (0 \le x \le 4.4).$$

The initial discharge and charge capacities of SnO_2 hollow spheres and double-void-space SnO_2/carbon composite are found to be 1478.9, 760.7 mAh g^{-1} and 1364.4, 697.4 mAh g^{-1}, respectively. The large initial irreversible losses can therefore be calculated to be 48.5% for SnO_2 and 48.9% for SnO_2/carbon composite. The primary reasons for this phenomenon include the following two aspects: the irreversible reduction of SnO_2 to Sn and the formation of the solid electrolyte interface (SEI) film. Fig. 5c depicts the cycling performance of both samples up to 50 cycles. The capacity of the 50th cycle is found to be 408.4 mAh g^{-1} for the double-

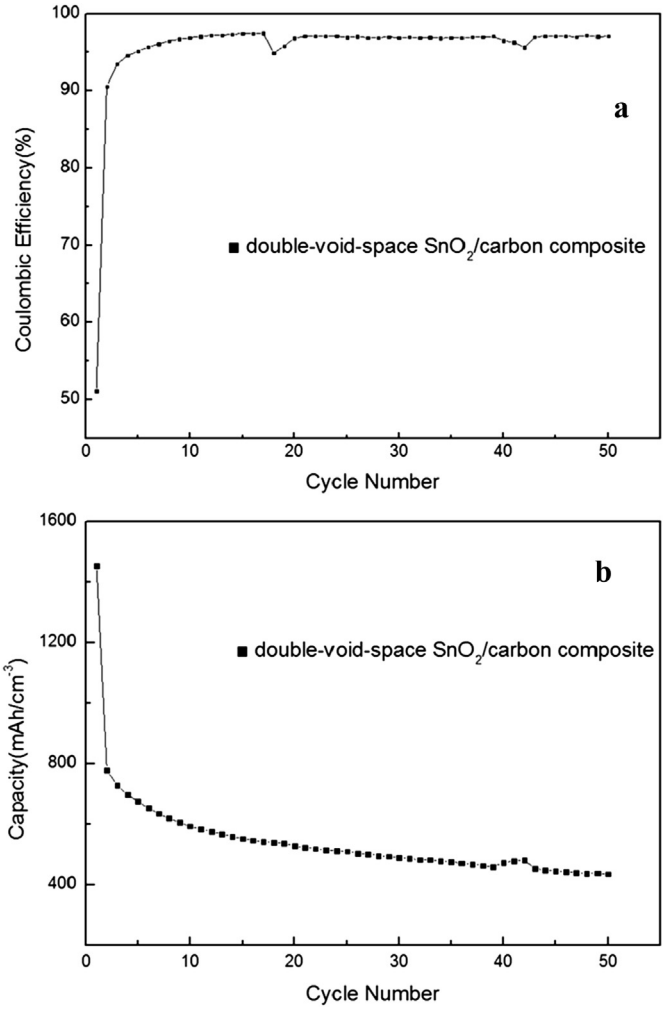

Fig. 6. (a) Coulombic efficiency of SnO_2/carbon composite at a density of 100 mA g^{-1}, (b) volumetric capacities of SnO_2/carbon composite at a current density of 100 mA g^{-1}.

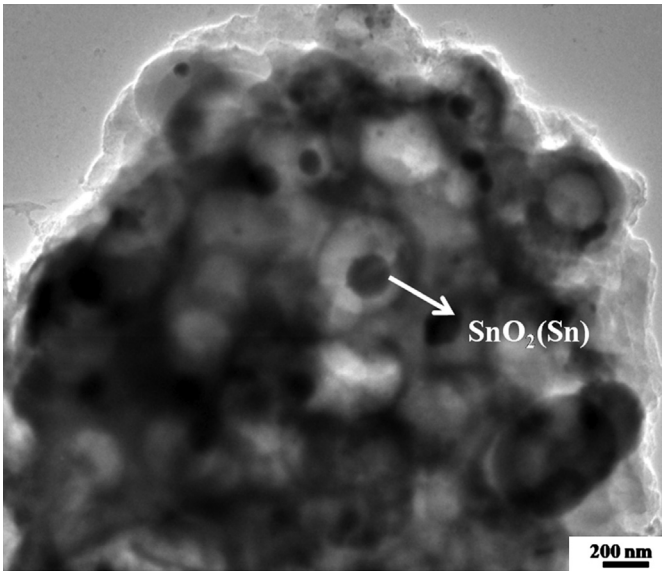

Fig. 7. HRTEM image of SnO_2/carbon composite after 50 cycles at a current density of 100 mA g^{-1}.

void-space SnO_2/carbon composite, which is much higher than the sample of SnO_2 hollow spheres (129.8 mAh g^{-1}). Considering of the carbon content (24.9 wt%) in the composite, we can calculate its theoretical specific capacity (685.42 mAh g^{-1}). After 50th cycle, the capacity of the composite still retains 59.6% of its theoretical specific capacity. In our paper, We have observed the phenomenon that the capacity retention of the samples is relatively similar to each other. The possible reasons: the carbon black and the residual capacity of SnO_2 itself make the hollow SnO_2 particles have a capacity of about 100 mAh g^{-1} even after 30th cycle [13,28]; the sample of the double-void-space composite is relatively stable of about 500 mAh g^{-1} after 30th cycle, which makes the tendency similar to the sample of SnO_2. Fig. 6a shows the coulombic efficiency of the double-void-space SnO_2/carbon composite in the 50 cycles. The coulombic efficiency of this composite is found to be larger than 92% from the second cycle and reach to about 97% in the 50th cycle. However, the irreversible capacity is still observed after the 1st cycle. There are two major reasons for this phenomenon: the irreversible reductive reaction between SnO_2 and Li is still taking place after the 1st cycle [28]; the continuous tiny pulverization of tin-based materials is still happened through subsequent cycles.

Fig. 6b shows the volumetric capacities of resulting materials. Because of the double-void-space structure, the electrode compacted density of double-void-space composite is 1.065 g cm^{-3}, which is a little lower than graphite (1.5 g cm^{-3}). The volumetric capacities of the 1st and 2nd cycle are found to be 1453.1 mAh cm^{-3} and 777.5 mAh cm^{-3}, which is much higher than that of graphite (558 mAh cm^{-3}). Even after 50 cycles at current rate of 100 mA g^{-1}, the capacity of the double-void-space SnO_2/carbon composite still remains 434.9 mAh cm^{-3}.

This double-void-space microstructure leads to several advantages. Firstly, the SnO_2 spheres have a very large internal void space. This hollow structure can partially accommodate the large volume change during the charge/discharge procedure according to many recent works. Secondly, the exterior void space between carbon and SnO_2 spheres can provide a buffer layer after the formation of Li_xSn. This special void space makes every pore to be a "minicell" and prevents the SnO_2 spheres extruding each other. As expected, the designed double-void-space SnO_2/carbon composite manifest exceptional electrochemical performance even after 50 cycles. Fig. 7 is a typical TEM image of the electrode after 50 cycles at current rate of 100 mA g^{-1}. The image is obscure due to the existence of the SEI layer. It is worth noting that the structure of "minicell" is still intact after electrochemical cycling and the SnO_2 (Sn) particles in each "cell" are trapped inside void space, which makes the resulting anode material have a stable and high capacity.

4. Conclusions

In summary, we have designed a new microstructured SnO_2/carbon composite anode material with the double-void-space structure for lithium-ion batteries. The formation of SnO_2 hollow spheres with large interior void space is based on an inside-out Ostwald ripening mechanism without templates. Furthermore, we used a modified Stöber method to synthesize the SiO_2 layer, which can switch to the exterior void space of the composite. The double-void-space structured materials displayed very satisfying results in both the performance of specific capacity and cycle life. Moreover, the preparation strategy we designed was easily transferable to other cathode, anode or supercapacitor materials by changing the core SnO_2 spheres.

References

[1] J.M. Tarascon, M. Armand, Nature 414 (2001) 358.
[2] K.T. Nam, D.W. Kim, P.J. Yoo, C.Y. Chiang, N. Meethong, P.T. Hammond, Y.M. Chiang, A.M. Belcher, Science 312 (2006) 885.
[3] J. Hassoun, S. Panero, P. Simon, P.L. Taberna, B. Scrosati, Adv. Mater. 276 (2007) 1395.
[4] W.J. Lee, M.H. Park, Y. Wang, J. Cho, Chem. Commun. 46 (2010) 622.
[5] C.K. Chan, H.L. Peng, G. Liu, Y. Cui, Nat. Nanotechnol. 3 (2008) 31.
[6] B. Koo, H. Xiong, M.D. Slater, E.V. Shevchenko, Nano Lett. 12 (2012) 2429.
[7] Y.J. Fu, X.W. Li, X.L. Sun, X.H. Wang, D.Q. Liu, D.Y. He, J. Mater. Chem. 22 (2012) 17429.
[8] J.Z. Wang, N. Du, H. Zhang, J.X. Yu, D. Yang, J. Phys. Chem. C 115 (2011) 11302.
[9] M. Winter, J.O. Besenhard, Electrochim. Acta 45 (1999) 31.
[10] I.A. Courtney, J.R. Dahn, J. Electrochem. Soc. 144 (1997) 2045.
[11] D. Larcher, S. Beattie, M. Morcrette, J.C. Jumas, J.M. Tarascon, J. Mater. Chem. 17 (2007) 3759.
[12] X.W. Lou, Y. Wang, C.L. Yuan, J.Y. Lee, L.A. Archer, Adv. Mater. 18 (2006) 2325.
[13] Y. Wang, J.Y. Lee, H.C. Zeng, Chem. Mater. 17 (2005) 3899.
[14] Z.Y. Wang, D.Y. Luan, X.W. Lou, J. Am. Chem. Soc. 133 (2011) 4738.
[15] L.B. Chen, X.M. Yin, T.H. Wang, Nanotechnology 23 (2012) 035402.
[16] G. Derrien, J. Hassoun, S. Panero, B. Scrosati, Adv. Mater. 19 (2007) 2336.
[17] Y. Wang, M.H. Wu, Z. Jiao, J.Y. Lee, Chem. Mater. 21 (2009) 3215.
[18] R.B. Ma, Y.B. Fu, X.H. Ma, Acta Phys. Chim. Sin. 25 (2009) 441.
[19] X. Wang, X.Q. Cao, L. Bourgeois, H. Guan, Y. Bando, D. Golberg, Adv. Funct. Mater. 22 (2012) 2682.
[20] Z.H. Wen, Q. Wang, Q. Zhang, J.H. Li, Adv. Funct. Mater. 17 (2007) 2772.
[21] S.H. Ng, J.Z. Wang, D. Wexler, K. Konstantinov, Z.P. Guo, H.K. Liu, Angew. Chem. Int. Ed. 45 (2006) 6896.
[22] M.S. Park, S.A. Needham, G.X. Wang, Y.M. Kang, J.S. Park, H.K. Liu, Chem. Mater. 19 (2007) 2406.
[23] W.M. Zhang, J.S. Hu, Y.G. Guo, S.F. Zheng, L.S. Zhong, W.G. Song, L.J. Wan, Adv. Mater. 20 (2008) 1160.
[24] W. Stöber, A. Fink, J. Colloid Interface Sci. 26 (1968) 62.
[25] J.S. Chen, C.M. Li, W.W. Zhou, X.W. Lou, Nanoscale 1 (2009) 280.
[26] W.R. Zhao, H.R. Chen, L.M. Guo, Q.J. He, F. Chen, J.L. Shi, ACS Nano 4 (2010) 529.
[27] R. Demir-Cakan, Y.S. Hu, M. Antonietti, J. Maier, M.M. Titirici, Chem. Mater. 20 (2008) 1227.
[28] M.S. Park, G.X. Wang, H.K. Liu, Angew. Chem. Int. Ed. 46 (2007) 750.